Surface & Coatings Technology 314 (2017) 148–154

Contents lists available at ScienceDirect

Surface & Coatings Technology

journal homepage: www.elsevier.com/locate/surfcoat

Plasma-based chemical functionalization of graphene to control the thermal transport at graphene-metal interfaces

S.G. Walton [a,*], B.M. Foley [b], S.C. Hernández [a], D.R. Boris [a], M. Baraket [a], J.C. Duda [b], J.T. Robinson [c], P.E. Hopkins [b]

[a] Plasma Physics Division, Naval Research Laboratory, 4555 Overlook Ave. SW, Washington, DC 20375-5346, USA
[b] Department of Mechanical and Aerospace Engineering, University of Virginia, Charlottesville, VA 22904, USA
[c] Electronics Science and Technology Division, Naval Research Laboratory, 4555 Overlook Ave. SW, Washington, DC 20375-5346, USA

ARTICLE INFO

Article history:
Received 3 October 2016
Revised 20 December 2016
Accepted in revised form 21 December 2016
Available online 29 December 2016

Keywords:
Plasma
Electron beam
Chemical functionalization
Graphene
Thermal transport

ABSTRACT

The unique characteristics of graphene have generated much excitement due to its utility across a variety of applications. One of the principal issues inhibiting the development of graphene technologies pertains to difficulties in engineering high-quality metal contacts on graphene. In this regard, the thermal transport at the metal/graphene interface plays a significant role in the overall performance of devices. Here, we demonstrate the use of electron beam produced plasmas to chemically modify graphene and how these modifications can be used to tune the thermal transport across metal-graphene interfaces. We show that the operating conditions of the plasma can be adjusted to control the character and quantity of chemical moieties at the interface. Typically, when changes in the surface chemistry favor an increase in adhesion between the graphene and metal, the thermal boundary conductance can be notably improved. Interestingly, the conventional approach of adding a titanium "wetting layer" to improve metal adhesion did not improve the thermal boundary conductance at gold contacts.

Published by Elsevier B.V.

1. Introduction

As research continues to highlight the unique features of graphene and related materials, there remains a demand to develop industrially-scalable, processing approaches and device architectures that can bring them to market. Graphene-based electronics is an application space that is notably rich in challenges [1]. One of those, which has been considered for quite some time, is associated with metal contacts on graphene. In particular, improving the electrical contact resistance at [2] and heat transfer across [3] the metal-graphene interface is critical for device development. The latter motivates this work.

Heat flows through material as energy carried by electrons and/or phonons [4] and so, the thermal conductance across an interface depends on their transport across the boundary. In other words, the thermal conductance (or resistance) across an interface depends on how easily free carriers pass through and/or vibrational modes couple across the interface of two materials. Not surprisingly then, the heat flow across graphene-metal interfaces is dependent upon the type of metal [5,6] and will be strongly affected by the interfacial roughness, [3,7] the presence of chemical defects [8,9], the number of graphene layers [10], and the substrate on which graphene resides [11,12]. While both electrons and phonons participate in thermal transport broadly, in the case of graphene-metal interfaces, it is generally accepted that the thermal conductance is largely determined by phonons rather than electrons [3,7,13,14]. Thus, like other systems, [15,16] improving the bonding or adhesion between the graphene and metal contact should improve thermal transport.

In our previous works [8,9], we showed that chemical moieties located between the metal and graphene influence the thermal transport across metal-graphene interfaces. The chemical moieties were introduced via plasma functionalization using electron beam generated plasmas. Plasma-based processes are readily scalable to meet the demands of wafer-scale fabrication and thus, when paired with large-area graphene growth techniques [17,18], provide a path toward industrial-level production of graphene-based electronics. While many different plasma sources have been used to functionalize or process graphene [19,20], electron beam generated plasmas are well-suited for graphene processing as they are capable of providing large fluxes of very low energy ions [21], which is an important factor in avoiding the damage to delicate structures often associated with conventional discharge plasmas [22]. Thus, with the appropriate choice of operating conditions, the type and amount of functional groups can be introduced at the metal-graphene interface and used to regulate the cross-plane thermal conductance.

In this work, we demonstrate the connection between the plasma operating parameters and graphene functionalization using plasma/system diagnostics. Specifically, we show how increasing the pressure

* Corresponding author.
E-mail address: scott.walton@nrl.navy.mil (S.G. Walton).

http://dx.doi.org/10.1016/j.surfcoat.2016.12.085
0257-8972/Published by Elsevier B.V.

leads to an increase in species production and thus functional group density. Then, using new and previously published results, we examine the relationship between adhesion and thermal boundary conductance at metal-graphene interfaces. In particular, we explore the relationship between chemical modification, surface wettability, and thermal boundary conductance. The results indicate that, with the exception of hydrogen-functionalized graphene, thermal boundary conductance increases when the functionalization leads to a more hydrophilic graphene surface. We also show that interfacial titanium layers do not significantly enhance thermal boundary conductance.

2. Processing system and experimental approach

2.1. Plasma processing system

The large area plasma processing system (LAPPS) is NRL-developed technology that employs magnetically-collimated, sheet-like electron beams to generate similarly sized plasma sheets for use in materials processing [23,24]. A schematic of the processing system is shown in Fig. 1. The base configuration is relatively simple, consisting of an electron beam source, slotted anode, termination anode, sample holder, and magnetic field coils. While these components are considered critical, there is significant flexibility in their design and operation. Typically, 1–3 keV electron beams with current densities of 1–5 mA/cm^2 are used. Co-axial magnetic fields of 100–300 G are used to collimate the electron beam and thus improve uniformity along its length [25]. These parameters are sufficient to produce uniform plasma sheets compatible with typical wafer-scale systems (diameter ≤ 300 mm) operating at low pressures (<100 mTorr).

For the results described here, the plasma processing system [26] and its operation for the processing of graphene [27,28,29,30] has been previously described in detail. Briefly, the system vacuum was maintained by a 250 l/s turbo pump, with a base pressure ~10^{-6} Torr. The operating pressure was achieved by introducing Ar (purity > 99.9999%) and reactive gas of choice (purity >99.999%) through the mass flow controllers and throttling the pumping speed using a manual gate valve. The reactive gas flow was always 5% of the total flow.

The electron beam was produced by applying a −2 kV pulse to a linear hollow cathode for a duration of 2 ms at a frequency of 50 Hz. The emergent beam passed through a slot in a grounded anode, traversed the gas, and was then terminated at a second grounded anode located further downstream. The electron beam volume between the two anodes defines the ionization source volume, with the dimensions set by the slot size (1 × 25 cm^2) and the anode-to-anode length (40 cm). A magnetic field of 150 G was produced by a set of external coils. The samples were placed on a 10.2 cm diameter stage located 3.0 cm from the electron beam axis. The stage was ground and held at room temperature.

The details of sample preparation can be found in refs [8,9]. Succinctly, single layer graphene was grown via low-pressure chemical vapor deposition (CVD) on copper foil [31] and transferred to 300 nm SiO_2/Si substrates via a standard wet chemical transfer technique [32]. Following transfer, the samples are assessed for quality and cleanliness and only those deemed sufficient were used for further study. For plasma processing, multiple samples were processed at each condition, where at least one is used for surface characterizations and the other was then metalized using e-beam evaporation. For this work, we examine both aluminum and gold contacts but in each case the thickness is 90 nm. For comparison, sets of sample that were not plasma functionalized as well as those prepared with a thin (2 nm) titanium (Ti) wetting layer were also metalized.

2.2. Plasma diagnostics

The plasma characterization experiments utilized a separate reactor dedicated for such efforts. The details of that system can be found in previous work [33,34]. It is worth noting however, that the diagnostic reactor utilizes a cylindrical electron beam that runs continuously, rather than a sheet electron beam that is pulsed. Although there will be some differences between the two systems, the important physics will be similar. All other conditions were nominally the same so that the general trends can be compared. Of interest are the bulk plasma characteristics as a function of operating conditions and to accomplish this, Langmuir probe measurements were performed using previously described data acquisition [33,34] and analysis [35] techniques,

2.3. Surface characterizations

Ex-situ surface diagnostics were performed using an X-ray photoelectron spectroscopy (K-Alpha XPS) system to identify the presence or absence of chemical elements. Surface composition was determined by fitting the high resolution elemental spectra of the C1s, F1s, N1s, O1s, etc. peaks using commercially available Unifit software. In the case of hydrogen functionalization, coverage was estimate by comparing the sp^2/sp^3 ratio in the C1s peak. The concentration of primary amines was determined using chemical tagging with a fluorine-containing molecule, which is readily quantified by XPS [27].

Static contact angle measurements were performed using an automated digital goniometer (AST Products, Inc.) equipped with a dispersing needle holder. Liquids with known surface properties (water, ethylene glycol, and diiodomethane) were placed on the graphene with a micro-syringe dedicated for each liquid. Once the micro-syringe is inserted in the needle holder, a 1 μl droplet is extruded while the graphene is raised perpendicular to the needle holder. Contact angles of both sides of three independent drops were averaged for each sample. As a reference, the water contact angle on uniform, as-transferred graphene is found to be ≈90°–100°. Contact angles typically vary by

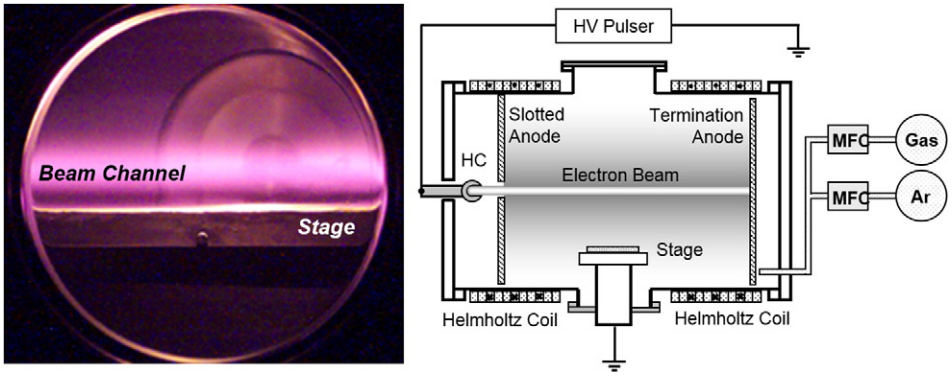

Fig. 1. The large area plasma processing system (LAPPS), which employs an electron beam generated plasma. (Left) An image of the plasma, and (Right) a schematic diagram of the processing reactor used in this work.

no more than ±2.0°. The surface energy was estimated using the Van Oss-Chaudhury-Good model [36].

2.4. Thermal boundary conductance

The thermal boundary conductance across the metal/graphene interfaces was measured with time domain thermoreflectance (TDTR) [4,37,38,39,40]. Much of the specific procedures and results reported here are detailed in our previous works [8,9]. TDTR is a pump-probe technique that relies on the principle of thermoreflectance of materials [41,42,43,44,45] to relate the measured change in reflectivity at the surface of a material to the transient change in temperature as a function of time after an ultrafast pump heating event. By utilizing ultrafast laser sources (sub-picosecond) and mechanical delay stages during a TDTR measurement, the thermoreflectance signal can be monitored with temporal resolution from <1 ps to several nanoseconds. This temporal "cooling curve" can then be related to a multilayer heat equation to determine the various thermal properties of the sample of interest. Given the ultrafast temporal resolution in a typical TDTR experiment, the sensitivity to heat transport on the nanoscale is high enough to measure the thermal conductivity of materials with length scales less than one-micron and the thermal boundary conductance across material interfaces. For example, it takes ≈100 ps for heat to diffusive across a 100 nm film with relatively high thermal conductivity (such as Al or Si), and ~1 ns for heat to effuse from one nanomaterial to another across an interface [46,47]. This is well within the capabilities of a typical TDTR experiment utilizing sub-picosecond pulses.

To provide more quantitative detail, Fig. 2a shows a schematic of the major components of a typical TDTR layout. Our specific TDTR set-up is utilizes a Ti:Sapph oscillator with ≈90 fs pulses centered around 800 nm emanating at an 80 MHz repetition rate. The pulse energy emerging from the laser cavity is split with a variable beam splitter into a pump path and a probe path. The pump beam is modulated by an electro-optic modulator (E.O. Modulator) driven by a linearly-amplified 11.39 MHz sinusoid, and then converted to 400 nm wavelength light using a BiB_3O_6 (BiBO) crystal, [48,13] while the probe beam is sent down a mechanical delay stage to delay the arrival of the probe relative to the pump at the sample surface. A photodiode and lock-in amplifier (SRS 844) are used to monitor the ratio of the in-phase (V_{in}) and out-of-phase (V_{out}) signals from the reflected probe beam at the modulation frequency of the pump. This ratio is monitored as a function of delay time to construct the "cooling curve" shown in Fig. 2b. This data set (TDTR ratio as a function of pump-probe delay time) is then related to a multi-layer thermal model accounting for modulated heating from a pulsed laser source and accumulation of thermal energy from the pulses, as described in detail in several references [4,37,38,39,40].

The thermoreflectance signals acquired using TDTR were fit to a two layer model (90 nm metals on semi-infinite SiO_2) to extract the thermal boundary conductance between the metal and SiO_2. The decision to treat the SiO_2 layer as semi-infinite is valid due to the extremely shallow thermal penetration depth of the thermal wave in this case. Due to the low thermal conductivity of the SiO_2 ($KSiO_2 = 1.28\ W\ m^{-1}\ K^{-1}$ at room temperature) [49] and the 11.39 MHz modulation frequency of the pump beam, the thermal penetration depth (δ) in this particular instance is approximately 150 nm. As a result, the thermal wave induced by the modulated pump beam will only propagate about half way into the 300 nm layer of SiO_2 and the modulated TDTR response will not be sensitive to the Si substrate, nor to the interface conductance between the SiO_2 and Si. Three TDTR scans were performed on each sample in the study to account for measurement uncertainty, and an additional uncertainly of ±3 nm in the thickness of the 90 nm metal transducer layer was included when fitting the TDTR data to the multilayer thermal model.

When fitting the data to the model, the SiO_2 was fixed at its literature value and the only free parameter was the metal/SiO_2 thermal boundary conductance, which includes the graphene monolayer. However, any contribution from the atomically-thin graphene sheet is assumed negligible, which has been confirmed in previous works [50,9]. The value extracted from the fit is actually an effective conductance which is a sum of the contributions from the interfaces on either side of the graphene, given by,

$$h_{K,metal/SLG/SiO2} = \left(h^{-1}_{K,metal/SLG} + h^{-1}_{K,SLG/SiO2}\right)^{-1} \quad (1)$$

where h_K is the thermal boundary conductance, or Kapitza conductance, at each interface [51,52,53]. From the measured total conductance and the literature value for the thermal boundary conductance at an SLG/SiO_2 interface (≈85 MW $m^{-2}\ K^{-1}$) [11], Eq. (1) can be used to determine the conductance across the functionalized metal/SLG interfaces.

3. Results and discussion

3.1. Plasma characterization and processing

In plasmas formed by injecting high-energy electron beams into a gas background, the basic inelastic processes leading to species production – ionization, dissociation, and excitation – are the same as those in discharge plasmas commonly used for processing. However, the resulting species densities and energies can be significantly different [21] due to the large difference in energies of the electrons that drive production. In typical discharges, species are produced by a low energy distribution of plasma electrons (T_e ≈ few eV) that have been heated

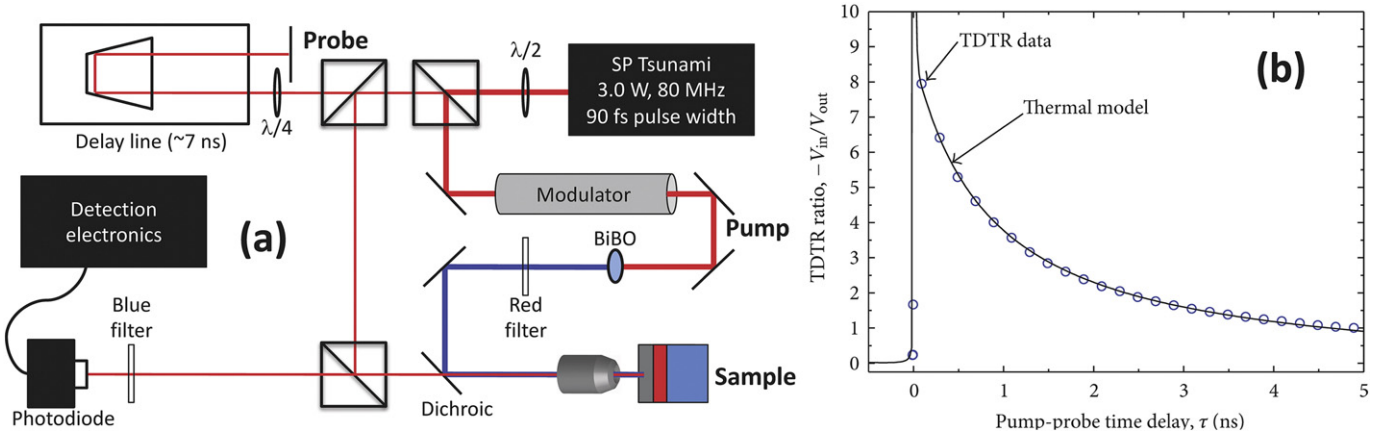

Fig. 2. (a) Major components in the TDTR experiments as described in the text along with (b) example TDTR data.

via an applied electric field to overcome the elastic and inelastic electron collisions that reduce their energy, such that some fraction of the resulting electron population is energetic enough to sustain the plasma through ionization. In contrast, species production in electron beam generated plasmas is largely due to high-energy beam electrons (E_{beam} ~ keV) and, in the absence of externally applied electric fields, plasma electrons rapidly cool to very low energies ($T_e \leq 1$ eV). As a result, one finds very different species production rates and relative species densities which leads to a unique flux of photons, chemically active species, and ions at adjacent surfaces.

The production of species via energetic electron beams can be written as,

$$S_i = k\, J_b N_i \sigma_i \tag{2}$$

where J_b is the beam current density, N_i is the number density of the parent molecule or atom, σ_i is the cross section for species production (for a given beam energy), and k is a proportionality coefficient [21]. There are several important implications derived from Eq. (2) that distinguish electron beam produced plasmas from their discharge counterparts. Relevant to this work, however, is the fact that a given species production will be proportional to the relative density of its parent molecule or atom and beam current. The results of Fig. 3 illustrate this point.

The cathode current, show in Fig. 3a, depends on both the type of reactive gas used and the operating pressure. The differences between gases is assumed to be related to differences in ion-induced secondary emission [54] and the rich gas-phase kinetics associated with the different reactive gas backgrounds. Importantly, the cathode current increases as function operating pressure, regardless of the gas type. If we assume the beam current scales with cathode current [26], then one would expect the production of species to increase more than linearly with pressure.

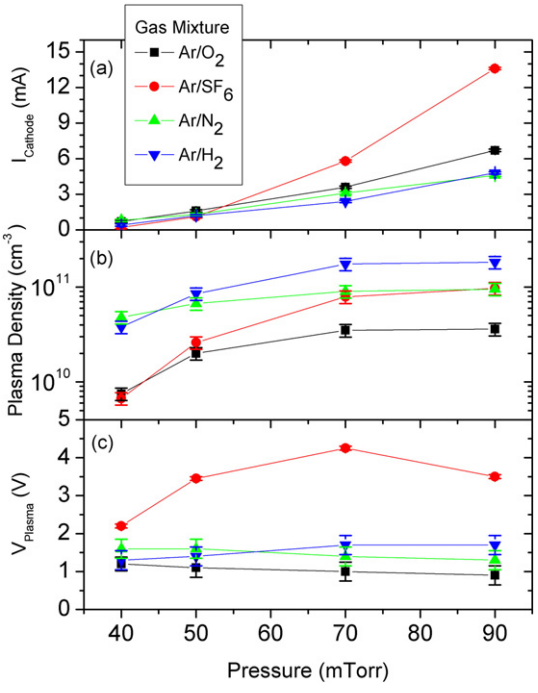

Fig. 3. Characteristics of electron beam generated plasmas produced in a variety of gas mixtures as a function of operating pressure. The indicated reactive gas is 5% by flow. Shown are (a) the cathode current along with corresponding (b) charged particle density and (c) plasma potential. The increase in plasma density and minimal change in plasma potential with pressure suggest and increase in ion and reactive neutral flux at the surface but no change in ion energy as pressure increases.

The plasma density, shown in Fig. 3b, evolves according to the continuity equation, which for a steady state plasma is given by,

$$-D_i \nabla^2 n_i = S_i - L_i \tag{3}$$

where D_i is the diffusion coefficient, n_i is the density, S_i is the source term, and L_i is the loss term. While diffusion to the walls determines the evolution of noble gas plasmas, gas-phase reactions dominate the evolution of plasmas produced in backgrounds containing even small amounts of molecular gases [55]. Thus, ones finds that charge exchange, electron-ion recombination, electron attachment, etc., included in the production and loss terms on the RHS of Eq. (3) are responsible for the spatio-temporal profiles of the charged particles. And so, while the plasma density generally increases with increasing pressure, it does not do so in a linear manner. Also note that the production of reactive radicals is expected to increase with increasing pressure since they too are created via the high energy electron beam [56,57]. While a full accounting of all the species and a detailed understanding of their evolution are important, the point of the results are that the production of charged and neutral plasma species increase as the pressure increases.

Lastly, the results of Fig. 3c show that, the plasma potential is low and independent of the operating conditions for all mixtures except Ar/SF_6. Although it does vary by a factor of two in that mixture, it remains below 4.5 V. Thus, while the flux of plasma species at a surface will increase with increasing pressure, the energy of the ions at the surface will not exceed 5 eV [21]. Ions with energies of this magnitude are well below that required to disrupt graphite [27] but sufficient to stimulate surface reactions [20].

Taken together, the above results suggest that an appropriate "knob" to control the processing of material in this system is pressure, where elevating the pressure increases the dose of reactive species and energetic ions at the surface. Importantly, the dose can be controlled independent of ion energy. These concepts are reflected in the results shown in Fig. 4, where the relative concentration of functional groups on the surface of graphene increase with increasing operating pressure [8,27,29]. Here, the concentration of the particular functional group (as indicated in parenthesis) is derived from the XPS spectra. As expected, the structure of the graphene changes with the addition of chemical moieties, leading

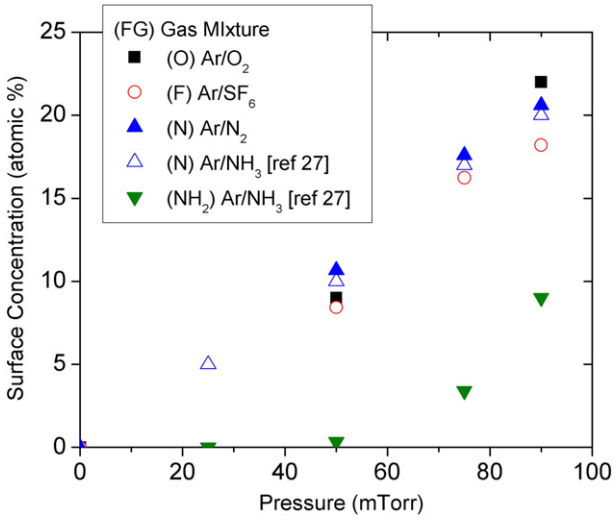

Fig. 4. The concentration of functional groups incorporated into the surface of graphene versus the operating pressure during plasma processing. The legend indicates the operating background gas (e.g. Ar/N_2) and associated functional group (e.g. N). Each functional group concentration was derived from XPS spectra. Like the plasma density in Fig. 3, the functional group concentration in each operating background is found to increase with increasing operating pressure. The results indicate functional group concentration on the surface is related to flux at the surface.

to, for example, a transition from sp^2 to sp^3 hybridization. While the degree of perturbation increases with increasing coverage [28,30], no erosion or etching of the carbon backbone has been observed for the conditions used here. A detailed analysis of the C1s high-resolution spectra as well as Raman spectra for O-, N-, and F-functionalized graphene for select process conditions can be found in [8,28,29] while XPS survey spectra and Raman spectra for NH_2-functionalized graphene can be found in [27].

Although it is tempting to draw a detailed connection between the density measurements (Fig. 3b) and the final surface concentration in Fig. 4, the density measurement does not account for the rich variety of reactive neutrals and ions within the plasma, their transport to the surface and how each interacts with the surface. A detailed chemical and structural analysis of the surfaces indicate that the bonding characteristics evolve as the coverage increases [30], suggesting a set of surface reactions that are coverage dependent. As a specific example, consider the results for graphene exposed to Ar/NH_3 plasmas [27]. The amount of N-containing functional groups increases in a linear manner with pressure while the primary amine concentration does not, which cannot be simply understood in terms of increasing plasma density or flux to the surface. Nonetheless, the results clearly show that by using the appropriate reactive gas and operating pressure, it is possible to control the type and concentration of chemical moieties on the surface of graphene, which can be used to control the characteristics of the surface.

Graphene is inert and so increasing its reactivity toward other materials has been of interest. In the context of the work here, chemical functionalization can be used to modify the surface energy in an effort control the interaction with deposited thin films. Changes in measured contact angle and surface energy after functionalization are shown in Table 1. In previous work [28], the connection between contact angle, surface energy and adhesion in oxygen- and fluorine-functionalize graphene was investigated. The presence of oxygen yielded a more hydrophilic surface that was characterized by a higher surface energy and adhesive forces. The addition of fluorine provided the opposite results; a hydrophobic surface with lower surface energy and adhesive forces.

The results of Table 1 show fluorination to be unique in the ability to create a more hydrophobic surface. Indeed, water contact angles are lower and surface energy higher when O, N, H, and NH_2 moieties are present. The values depend on the functional group type and, while the hydrogen coverage is not well known, the trends agree with previous work [27] showing an increase in hydrophilicity with coverage. Thus, with the exception of fluorine, chemical modification is expected to promote the adhesion of metal films.

3.2. TDTR and the management of thermal conductance

In our previous works, we have studied the influence of functional groups, introduced via plasma processing, on the thermal boundary conductance across graphene-aluminum [9] and graphene-gold [8] interfaces. Those results are summarized in Fig. 5 for samples at room temperature. Both Al and Au are expected to be physisorbed on the surface of graphene, which is theorized to results in a lower thermal boundary conductance compared to chemisorbed systems, such as Ni- and Ti-graphene [5,6,10]. From this, one can reasonably assume that the addition of functional groups that lead to a more hydrophilic surface, a typical indicator of improved adhesion between the metal film and graphene, should increase the thermal boundary conductance. The results of Fig. 5 generally support this concept where the addition of oxygen and nitrogen moieties increase the thermal boundary conductance and that increase depends on the amount of those groups. In fact the, increase in conductance appears to be less dependent on functional group type and more on surface concentration. The presence of fluorine-containing groups, which make the surface slightly more hydrophobic, have no effect on the thermal boundary conductance.

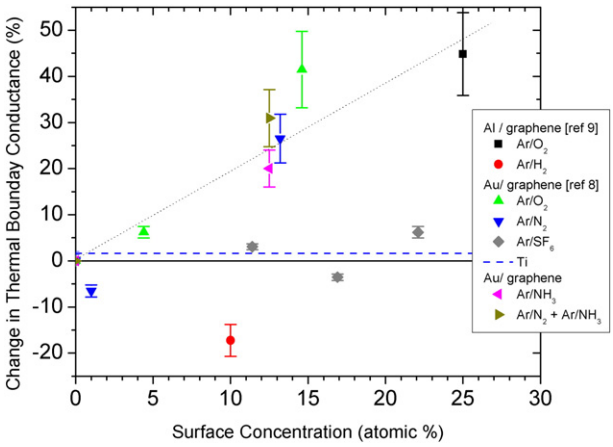

Fig. 5. The change in thermal boundary conductance at aluminum-graphene (Al/Gr) and gold-graphene (Au/Gr) interfaces as a function of the type and concentration of functional groups at the interface prepared using operating backgrounds indicated in the legend (e.g. Ar/O_2). The functional groups incorporated will be the same as in Fig. 4, with the ammonia treatments introducing some mixture of N and NH_x groups. Also shown (dashed line) is the result for an interface prepared using a Ti thin film (i.e. Au/Ti/Gr). The presence of H- and F-functional groups as well as the Ti layer has little or negative impact on the thermal boundary conductance. The presence of O- and N-functional groups, however, tends to increase the thermal boundary conductance in proportion to the concentration of those groups (the dotted line).

The presence of hydrogen and its influence on thermal boundary conductance is interesting. When H is introduced via Ar/H_2 plasmas, the graphene is more hydrophilic and yet the thermal boundary conductance decreases. To understand this, subsequent studies using ammonia-containing plasmas to introduce H moieties were performed. In one case, an Ar/NH_3 plasma was used and in the second, a two-step Ar/N_2 plasma followed by an Ar/NH_3 was used. The results indicated that when hydrogen exists in the form of NH_2, both the hydrophilicity and thermal boundary conductance increase. The magnitude of which depends on the amount of nitrogen exposure.

The results for pure hydrogen functionalization are not well understood since hydrogen, like nitrogen and oxygen is found to make the surface more hydrophilic. In line with our contact angle measurements, numerical studies of graphane – fully hydrated graphene – have found it to be more hydrophilic than graphene [59,60]. As such, an increase, rather than decrease, in the measured thermal boundary conductance is expected. On the other hand, Monachon et al. [15] showed a decrease in thermal boundary conductance across the interface of Cu, Al, and Ni thin films and diamond substrates when the diamond is hydrogen terminated. In this case however, hydrogen termination was also found to lower the surface energy, as well as the work of adhesion between the metal and substrates. In other words, their results show a correlation between decreasing thermal boundary conductance and reduced adhesion in diamond.

It might well be that water contact angle and/or adhesion is not sufficient to predict the thermal boundary conductance in all cases. Given

Table 1
Change in water contact angle and surface energy for chemically modified graphene. With the exception of fluorinated graphene, the chemical modification of graphene produces a surface that is more hydrophilic and has a higher surface energy.

Plasma background	Operating pressure (mTorr)	Functional group	Surface coverage (%)	Δ H_2O contact angle (%)	Δ surface energy (%)	Ref
Ar/SF_6	50	F	12	2%	−39%	[28]
Ar/O_2	50	O	11	−70%	24%	[28]
Ar/N_2	50	N	8	−54%	16%	[29]
Ar/N_2	90	N	20	−40%	35%	
Ar/NH_3	90	NH_2	9	−40%	32%	
Ar/H_2	50	H	≈10	−18%	Unknown	
Ar/H_2	90	H	>20	−30%	Unknown	
H_2	Unknown	H	<5	−27%	42%	[58]

graphene's atomic thinness, the influence of the underlying substrate on wetting [61,62] and adhesive interactions [63] cannot be ignored. As such, the interfacial properties that most affect thermal boundary conductance, such as chemical bond formation (or lack of), might not be appropriately accounted for in the measurement. Even so, the character of the bonding between the metal and graphene is not always a good predictor of thermal boundary conductance. For example, Mao et al. [64] showed there might be exceptions to the aforementioned notion that thermal conductance is higher for chemisorbed metals.

Also shown in Fig. 5 is the change in conductance when a titanium wetting layer (2 nm) is used as an interfacial layer between graphene and Au. As noted above, Ti chemisorbs to graphene and based on theoretical works [10], should have a higher thermal boundary conductance than Au. And yet, when added to the interface, no significant change is observed. A possible explanation is that the thermal conductance measured across these structures could be dominated by the resistance of the thin Ti layer, the thermal conductivity of which could be quite reduced due to its thickness and any change in stoichiometry due to interactions during deposition on the graphene surface. Thus, similar to the example of hydrogen above, the use of Ti might improve the adhesion of metal films to graphene but does not appear to improve the overall thermal conduction between them.

4. Summary

In this work, we demonstrated a plasma-based method to engineer the thermal conductance across metal/graphene interfaces by manipulating the interface chemistry. Using simple changes in operating background and pressure, the character and quantity of chemical moieties at the interface can be varied to provide notable changes in the thermal boundary conductance. We find the introduction of nitrogen and oxygen functionalities, which are also shown to increase the hydrophilicity of the graphene, produce a significant increase in thermal boundary conductance. However, the introduction of hydrogen, which also increases the hydrophilicity, lowers the conductance. The addition of fluorine, which makes the graphene more hydrophobic, has little impact on the thermal boundary conductance. Interestingly, the conventional approach of adding a titanium "wetting layer" to improve metal adhesion did not improve the thermal boundary conductance. While the results for nitrogen and oxygen suggest a correlation between increased wettability or improved adhesion and higher thermal boundary conductance across metal/graphene interfaces, the broader results indicate a more detailed understanding of the interface chemistry and/or transport phenomena is needed before generalizing the relationship for metal/graphene systems. Nonetheless, the results suggest chemical functionalization via electron beam generated plasmas is an attractive route toward managing the thermal transport across metal/graphene interfaces.

Acknowledgment

This work was partially supported by the Naval Research Laboratory base program and the Office of Naval Research (Grant No. N00014-15-12769). M. Baraket acknowledges the support of the National Research Council.

References

[1] K. Asadi, E.C. Timmering, T.C.T. Geuns, A. Pesquera, A. Centeno, A. Zurutuza, J.H. Klootwijk, P.W.M. Blom, D.M. de Leeuw, Up-scaling graphene electronics by reproducible metal–graphene contacts, ACS Appl. Mater. Interfaces 7 (2015) 9429–9435.
[2] B.K. Bharadwaj, D. Nath, R. Pratap, S. Raghavan, Making consistent contacts to graphene: effect of architecture and growth induced defects, Nanotechnology 27 (2016) 205705–205706.
[3] B. Huang, Y.K. Koh, Improved topological conformity enhances heat conduction across metal contacts on transferred graphene, Carbon 105 (2016) 268–274.
[4] D.G. Cahill, K. Goodson, A. Majumdar, Thermometry and thermal transport in micro/nanoscale solid-state devices and structures, J. Heat Transf. 124 (2001) 223–241.
[5] T. Wejrzanowski, M. Grybczuk, M. Wasiluk, K.J. Kurzydlowski, Heat transfer through metal-graphene interfaces, AIP Adv. 5 (2015) 077142.
[6] R. Mao, B.D. Kong, C. Gong, S. Xu, T. Jayasekera, K. Cho, K.W. Kim, First-principles calculation of thermal transport in metal/graphene systems, Phys. Rev. B 87 (2013) 165410.
[7] Y. Hong, L. Li, X.C. Zeng, J. Zhang, Tuning thermal contact conductance at graphene–copper interface via surface nanoengineering, Nanoscale 7 (2015) 6286.
[8] B.M. Foley, S.C. Hernández, J.C. Duda, J.T. Robinson, S.G. Walton, P.E. Hopkins, Modifying surface energy of graphene via plasma-based chemical functionalization to tune thermal and electrical transport at metal interfaces, Nano Lett. 15 (2015) 4876.
[9] P.E. Hopkins, M. Baraket, E.V. Barnat, T.E. Beechem, S.P. Kearney, J.C. Duda, J.T. Robinson, S.G. Walton, Manipulating thermal conductance at metal–graphene contacts via chemical functionalization, Nano Lett. 12 (590) (2012).
[10] L. Chen, Z. Huang, S. Kumar, Impact of bonding at multi-layer graphene/metal interfaces on thermal boundary conductance, RSC Adv. 4 (2014) 35852–35861.
[11] Z. Chen, W. Jang, W. Bao, C.N. Lau, C. Dames, Thermal contact resistance between graphene and silicon dioxide, Appl. Phys. Lett. 95 (2009) 161910.
[12] Z.-Y. Ong, E. Pop, Effect of substrate modes on thermal transport in supported graphene, Phys. Rev. B 84 (2011) 075741.
[13] Y.K. Koh, M.-H. Bae, D.G. Cahill, E. Pop, Heat conduction across monolayer and few-layer graphenes, Nano Lett. 10 (11) (2010) 4363–4368.
[14] J. Zhang, F. Xu, Y. Hong, Q. Xiong, J. Pan, A comprehensive review on the molecular dynamics simulation of the novel thermal properties of graphene, RSC Adv. 5 (109) (2015) 89415–89426.
[15] C. Monachon, G. Schusteritsch, E. Kaxiras, L. Weber, Qualitative link between work of adhesion and thermal conductance of metal/diamond interfaces, J. Appl. Phys. 115 (2014) 123509.
[16] M.D. Losego, M.E. Grady, N.R. Sottos, D.G. Cahill, P.V. Braun, Effects of chemical bonding on heat transport across interfaces, Nat. Mater. Lett. 11 (2012) 502.
[17] Y. Li, N. Chopra, Progress in large-scale production of graphene. Part 1: chemical methods, JOM 67 (2015) 34–43.
[18] Y. Li, N. Chopra, Progress in large-scale production of graphene. Part 2: vapor methods, JOM 67 (1) (2015) 44–52.
[19] A. Dey, A. Chroneos, N.S.J. Braithwaite, R.P. Gandhiraman, S. Krishnamurthy, Plasma engineering of graphene, Appl. Phys. Rev. 3 (2016) 021301.
[20] K. Ostrikov, E.C. Neyts, M. Meyyappan, Plasma nanoscience: from nano-solids in plasmas to nano-plasmas in solids, Adv. Phys. 62 (2) (2013) 113–224.
[21] S.G. Walton, D.R. Boris, S.C. Hernández, E.H. Lock, T.B. Petrova, G.M. Petrov, R.F. Fernsler, Electron beam generated plasmas for ultra low Te processing, ECS J. Solid State Sci. Technol. 4 (6) (2015) N5033–N5040.
[22] A.V. Jagtiani, H. Miyazoe, J. Chang, D.B. Farmer, M. Engel, D. Neumayer, S.-J. Han, S.U. Engelmann, D.R. Boris, S.C. Hernández, E.H. Lock, S.G. Walton, E.A. Joseph, Initial evaluation and comparison of plasma damage to atomic layer carbon materials using conventional and low Te plasma sources, J. Vac. Sci. Technol. A 34 (2016) 01B103.
[23] W.M. Manheimer, R.F. Fernsler, M. Lampe, R.A. Meger, Theoretical overview of the large-area plasma processing system (LAPPS), Plasma Sources Sci. Technol. 9 (2000) 370–386.
[24] R.A. Meger, R.F. Fernsler, M. Lampe, W. Manheimer, "Large Area Plasma Processing System," U.S. Patent 5,874,807, Feb 23, 1999.
[25] G.M. Petrov, D.R. Boris, E.H. Lock, T.B. Petrova, R.F. Fernsler, S.G. Walton, The influence of magnetic field on electron beam generated plasmas, J. Phys. D. Appl. Phys. 48 (2015) 275202–275208.
[26] S.G. Walton, E.H. Lock, A. Ni, M. Baraket, R.F. Fernsler, D.D. Pappas, K.E. Strawhecker, A.A. Bujanda, Study of plasma-polyethylene interactions using electron beam generated plasmas produced in Ar/SF6 mixtures, J. Appl. Polym. Sci. 117 (3515) (2010).
[27] M. Baraket, R. Stine, W.K. Lee, J.T. Robinson, C.R. Tamanaha, P.E. Sheehan, S.G. Walton, Aminated graphene for DNA attachment produced via plasma functionalization, Appl. Phys. Lett. 100 (2012) 233123.
[28] S.C. Hernández, C.J.C. Bennett, C.E. Junkermeier, S.D. Tsoi, F.J. Bezares, R. Stine, J.T. Robinson, E.H. Lock, D.R. Boris, B.D. Pate, J.D. Caldwell, T.L. Reinecke, P.E. Sheehan, S.G. Walton, Chemical gradients on graphene to drive droplet motion, ACS Nano 7 (6) (2013) 4746–4755.
[29] S.C. Hernández, F.J. Bezares, J.T. Robinson, J.D. Caldwell, S.G. Walton, Controlling the local chemical reactivity of graphene through spatial functionalization, Carbon 60 (2013) 84–93.
[30] S.C. Hernández, V.D. Wheeler, M.S. Osofsky, V.K. Nagareddy, E.H. Lock, L.O. Nyakiti, R.L. Myers-Ward, A.B. Horsfall, C.R. Eddy Jr., D.K. Gaskill, S.G. Walton, Plasma-based chemical modification of epitaxial graphene with oxygen functionalities, Surf. Coat. Technol. 241 (2014) 8.
[31] X. Li, C.W. Magnuson, A. Venugopal, R.M. Tromp, J.B. Hannon, E.M. Vogel, L. Colombo, R.S. Ruoff, Large-area graphene single crystals grown by low-pressure chemical vapor deposition of methane on copper, J. Am. Chem. Soc. 133 (2011) 2816–2819.
[32] K.S. Kim, Y. Zhao, H. Jang, S.Y. Lee, J.M. Kim, J.H. Ahn, P. Kim, J.Y. Choi, B.H. Hong, Large-scale pattern growth of graphene films for stretchable transparent electrodes, Nature 457 (2009) 706–710.
[33] D.R. Boris, R.F. Fernsler, S.G. Walton, Measuring the density, electron temperature, and electronegativity in electron beam generated plasmas produced in argon/SF6 mixtures, Plasma Sources Sci. Technol. 24 (2015) 025032.
[34] D.R. Boris, G.M. Petrov, E.H. Lock, T.B. Petrova, R.F. Fernsler, S.G. Walton, Controlling the electron energy distribution function of electron beam generated plasmas with molecular gas concentration: part I. Experimental results, Plasma Sources Sci. Technol. 22 (2013) 065004–065006.
[35] R.F. Fernsler, Modeling Langmuir probes in multi-component plasmas, Plasma Sources Sci. Technol. 18 (2009) 014012.

[36] C.J. Van Oss, R.J. Good, M.K. Chaudhury, Additive and nonadditive surface-tension components and the interpretation of contact angles, Langmuir 4 (1988) 884–891.
[37] A.J. Schmidt, X. Chen, G. Chen, Pulse accumulation, radial heat conduction, and anisotropic thermal conductivity in pump-probe transient thermoreflectance, Rev. Sci. Instrum. 79 (2008) 114902.
[38] A.J. Schmidt, Pump-probe thermoreflectance, Ann. Rev. Heat Transf. 16 (2013) 159–181.
[39] P.E. Hopkins, J.R. Serrano, L.M. Phinney, S.P. Kearney, T.W. Grasser, C.T. Harris, Criteria for cross-plane dominated thermal transport in multilayer thin film systems during modulated laser heating, J. Heat Transf. 132 (2010) 081302.
[40] D.G. Cahill, Analysis of heat flow in layered structures for time-domain thermoreflectance, Rev. Sci. Instrum. 75 (2004) 5119–5122.
[41] R. Rosei, D.W. Lynch, Thermomodulation spectra of Al, Au, and Cu, Phys. Rev. B 5 (1972) 3883–3894.
[42] P.E. Hopkins, Effects of electron-boundary scattering on changes in thermoreflectance in thin metal films undergoing intraband excitations, J. Appl. Phys. 105 (2009) 093517.
[43] P.E. Hopkins, Influence of electron-boundary scattering on thermoreflectance calculations after intra- and interband transitions induced by short-pulsed laser absorption, Phys. Rev. B 81 (2010) 035413.
[44] P.E. Hopkins, Thermoreflectance dependence on Fermi surface electron number density perturbations, Appl. Phys. Lett. 96 (041901) (2010).
[45] Y. Wang, J.Y. Park, Y.K. Koh, D.G. Cahill, Thermoreflectance of metal transducers for time-domain thermoreflectance, J. Appl. Phys. 108 (2010) 043507.
[46] P.E. Hopkins, R.J. Stevens, P.M. Norris, Influence of inelastic scattering at metal-dielectric interfaces, J. Heat Transf. 130 (2008) 022401.
[47] R.J. Stoner, H.J. Maris, Kapitza conductance and heat flow between solids at temperatures from 50 to 300 K, Phys. Rev. B 48 (1993) 16373–16387.
[48] M. Ghotbi, M. Ebrahim-Zadeh, A. Majchrowski, E. Michalski, I.V. Kityk, High-average-power femtosecond pulse generation in the blue using BiB3O6, Opt. Lett. 29 (2004) 2530–2532.
[49] D.G. Cahill, Thermal conductivity measurement from 30 to 750 K: the 3ω method, Rev. Sci. Instrum. 61 (1990) 802–808.
[50] Y.K. Koh, M.-K. Bae, D.G. Cahill, E. Pop, Heat conduction across monolayer and few layer graphenes, Nano Lett. 10 (2010) 4363–4368.
[51] P.E. Hopkins, Thermal transport across solid interfaces with nanoscale imperfections: effects of roughness, disorder, dislocations, and bonding on thermal boundary conductance, ISRN Mech. Eng. 2013 (2013) 682586.
[52] E.T. Swartz, R.O. Pohl, Thermal boundary resistance, Rev. Mod. Phys. 61 (1989) 605–668.
[53] P.L. Kapitza, The study of heat transfer in helium II, Zhurnal eksperimentalnoi i teoreticheskoi fiziki 11 (1941) 1–31.
[54] S.G. Walton, D. Leonhardt, R.F. Fernsler, Hollow Cathode Produced Electron Beams for Plasma Generation: Cathode Operation in Gas Mixtures, NRL Internal Report No. NRL-MR-6750-8992, September 2006.
[55] D.R. Boris, R.F. Fernsler, S.G. Walton, The spatial profile of density in electron beam generated plasmas, Surf. Coat. Technol. 241 (13) (2014) 13–18.
[56] S.G. Walton, E.H. Lock, R.F. Fernsler, Plasma modification of solid and porous polyethylene, Plasma Process. Polym. 5 (453) (2008).
[57] G.M. Petrov, D.R. Boris, T.B. Petrova, S.G. Walton, One-dimensional Ar-SF6 hydromodel at low-pressure in e-beam generated plasmas, J. Vac. Sci. Technol. A 34 (2016) 021302–021312.
[58] C.J. Russo, L.A. Passmore, Controlling protein adsorption on graphene for cryo-EM using low-energy hydrogen plasmas, Nat. Methods 11 (6) (2014) 649–652.
[59] D. Umadevi, G.N. Sastry, Graphane versus graphene: a computational investigation of the interaction of nucleobases, aminoacids, heterocycles, small molecules (CO2, H2O, NH3, CH4, H2), metal ions and onium ions, Phys. Chem. Chem. Phys. 17 (2015) 30260–30269.
[60] D. Vanzo, D. Bratko, A. Luzar, Wettability of pristine and alkyl-functionalized graphane, J. Chem. Phys. 137 (2012) 034707.
[61] B. Ramos-Alvarado, S. Kumar, G.P. Peterson, On the wettability transparency of graphene-coated silicon surfaces, J. Chem. Phys. 144 (2016) 014701.
[62] D. Kim, N.M. Pugno, M.J. Buehler, S. Ryu, Solving the controversy on the wetting transparency of graphene, Sci. Report. 5 (2015) 15526.
[63] J.W. Suk, S.R. Na, R.J. Stromberg, D. Stauffer, J. Lee, R.S. Ruoff, K.M. Liechti, Probing the adhesion interactions of graphene on silicon oxide by nanoindentation, Carbon 103 (2016) 63–72.
[64] R. Mao, B.D. Kong, C. Gong, S. Xu, T. Jayasekera, K. Cho, K.W. Kim, First-principles calculation of thermal transport in metal/graphene systems, Phys. Rev. B 87 (2013) 165410.